Manganese(II/II/II) and Manganese(III/II/III) Trinuclear Compounds. Structure and Solid and Solution Behavior

Vasilis Tangoulis,[§] Dora A. Malamatari,[†] Kali Soulti,[‡] Voula Stergiou,[†] Catherine P. Raptopoulou,[§] Aris Terzis,[§] Themistoklis A. Kabanos,*[,‡] and Dimitris P. Kessissoglou*[,†]

Department of General & Inorganic Chemistry, Aristotle University of Thessaloniki, 54006 Thessaloniki, Greece, Department of Chemistry, Section of Inorganic and Analytical Chemistry, University of Ioannina, 45110 Ioannina, Greece, and NRCPS "Demokritos", Institute of Materials Science, 15310 Aghia Paraskevi Attikis, Greece

Received February 22, 1996[⊗]

Two mixed-valence $Mn^{III}Mn^{II}$ complexes and a homo-valence Mn^{II} trinuclear manganese complex of stoichiometry $Mn^{III}Mn^{II}Mn^{III}$(*5-Cl-Hsaladhp*)$_2$(AcO)$_4$(MeOH)$_2$·4CH_3OH (**1a**), $Mn^{III}Mn^{II}Mn^{III}$ (*Hsaladhp*)$_2$(AcO)$_2$(*5-Cl-Sal*)$_2$-(*thf*)$_2$ (**3a**) and $Mn^{II}Mn^{II}Mn^{II}$ (AcO)$_6$(*pybim*)$_2$ (**1b**) where *H$_3$saladhp* is a tridentate Schiff base ligand and *pybim* a neutral bidentate donor ligand, have been structurally characterized by using X-ray crystallography. The structurally characterized mixed-valence complexes have strictly 180° $Mn^{III}-Mn^{II}-Mn^{III}$ angles as required by crystallographic inversion symmetry. The complexes are valence trapped with two terminal Mn^{III} ions showing Jahn-Teller distortion along the acetate or salicylate−Mn^{III}−X axis. The Mn···Mn separation is 3.511 Å and 3.507 Å respectively. The mixed-valence complexes have $S = {}^3/_2$ ground state and the homovalence complex $S = {}^5/_2$, with small antiferromagnetic exchange J couplings, −5.6 and −1.8 cm^{-1}, respectively, while the powder ESR spectra at 4 K show a broad low field signal with $g \approx 4.3$ for $Mn^{III}Mn^{II}Mn^{III}$ and a broad temperature-dependent signal at $g = 2$ for $Mn^{II}Mn^{II}Mn^{II}$. Crystal data for **1a**: [$C_{36}H_{60}O_{20}N_2Cl_2Mn_3$], triclinic, space group $P\bar{1}$, $a = 9.272(7)$ Å, $b = 11.046(8)$ Å, $c = 12.635(9)$ Å, $\alpha = 76.78(2)°$, $\beta = 81.84(2)°$, $\gamma = 85.90(2)°$, $Z = 1$. Crystal data for **3a**: [$C_{48}H_{56}O_{18}N_2Cl_2Mn_3$], monoclinic, space group $P2_1/n$, $a = 8.776(3)$ Å, $b = 22.182(7)$ Å, $c = 13.575(4)$ Å, $\beta = 94.44(1)°$, $Z = 2$. Crystal data for **1b**: [$C_{36}H_{36}O_{12}N_6Mn_3$], triclinic, space group $P\bar{1}$, $a = 13.345(6)$ Å, $b = 8.514(4)$ Å, $c = 9.494(4)$ Å, $\alpha = 75.48(1)°$, $\beta = 75.83(1)°$, $\gamma = 76.42(1)°$, $Z = 1$.

Introduction

The chemistry of manganese has received considerable attention in recent years due to the fact that manganese is believed to be catalytically active in a variety of metalloenzymes.[1] One of the most important processes in nature occurs in the oxygen evolving complex (OEC) of photosystem II (PSII), where the four-electron oxidation of water to molecular oxygen is believed to be catalyzed by a cluster of four manganese ions.[2,3] The available data strongly suggest that a polynuclear cluster is responsible for the ESR detectable signals in the "active form" of S_1 ($g = 4.8$ in parallel polarization) and S_2 ($g = 2$ multiline and $g = 4.1$ with fine structure) oxidation states of the OEC.[4−10] In addition EXAFS data[11−13] indicate the presence of at least two ∼2.7 Å Mn···Mn interactions in addition to an ∼3.3 Å interaction. The manganese coordination sphere is believed to be dominated by O and N donors from available amino acid side chains.[14,15] Whereas considerable information is now available about the higher oxidation states of the polymanganese oxo centers through the study of model compounds, much less is known about the reduced 2+ state.[16−18] Attempts to reproduce the functional chemistry of metal centers in manganese proteins has drawn attention to di- and trivalent manganese.

Previous efforts have centered on the preparation and characterization of a variety of mononuclear, binuclear, and trinuclear complexes with predominantly oxygen-donor ligands in order to understand the fundamental coordination, structure, and magnetochemistry of complexes potentially relevant to the active site of the OEC.[19−27] A number of workers have prepared

[†] Aristotle University of Thessaloniki.
[‡] University of Ioannina.
[§] Institute of Materials Science.
[⊗] Abstract published in *Advance ACS Abstracts,* July 1, 1996.

(1) Pecoraro, V. L. *Manganese Redox Enzymes*; VCH Publishers Inc.: New York, 1992.
(2) Dismukes, G. C. *Photochem. Photobiol.* **1986**, *43*, 99.
(3) Pecoraro, V. L. *Photochem. Photobiol.* **1988**, *48*, 249.
(4) Dismukes, G. C.; Siderer, Y. *Proc. Natl. Acad. Sci. U.S.A.* **1981**, *78*, 274.
(5) Casey, J.; Sauer, K. *Biochem. Biophys. Acta.* **1984**, *767*, 21.
(6) dePaula, J. C.; Beck, W. F.; Brudving, G. W. *J. Am. Chem. Soc.* **1986**, *108*, 4002.
(7) Hansson, O. R.; Aasa, R.; Vanngard, T. *Biophys. J.* **1987**, *51*, 825.
(8) Zimmermann, J.-L.; Rutherford, A. W. *Biochemistry* **1986**, *25*, 4609.
(9) Kim, D. H.; Britt, R. D.; Klein, M. P.; Sauer, K. *Biochemistry* **1992**, *31*, 541.
(10) Dexheimer, S. L.; Klein, M. P. *J. Am. Chem. Soc.* **1992**, *114*, 2821.
(11) Guiles, R. D.; Yachandra, V. K.; McDermott, A. E.; Cole, J. L.; Dexheimer, S. L.; Britt, R. D.; Sauer, K.; Klein, M. P. *Biochemistry* **1990**, *29*, 486.
(12) George, G. N.; Prince, R. C.; Cramer, S. P. *Science* **1989**, *243*, 789.
(13) Penner-Hahn, J. E.; Fronko, R. M.; Pecoraro, V. L.; Yocum, C. F.; Betts, S. D.; Bowlby, N. R. *J. Am. Chem. Soc.* **1990**, *112*, 2549.
(14) Tamura, N.; Ikeuchi, M.; Inoue, Y. *Biochim. Biophys. Acta* **1989**, *973*, 281.
(15) Andreasson, L.-E. *Biochim. Biophys. Acta* **1989**, *973*, 465.
(16) Wieghardt, K. *Angew. Chem., Int. Ed. Engl.* **1989**, *28*, 1153.
(17) Vincent, J. B.; Christou, G. *Adv. Inorg. Chem. Radiochem.* **1989**, *33*, 197.
(18) Christou, G. *Acc. Chem. Res.* **1989**, *22*, 328.
(19) Kessissoglou, D. P.; Butler, W. M.; Pecoraro, V. L. *J. Chem. Soc., Chem. Commun.* **1986**, 1253.
(20) Kessissoglou, D. P.; Li, X.-H.; Butler, W. M.; Pecoraro, V. L. *Inorg. Chem.* **1987**, *26*, 2487.
(21) Li, X-H.; Kessissoglou, D. P.; Kirk, M. L.; Bender, C.; Pecoraro, V. L. *Inorg. Chem.* **1988**, *27*, 1.
(22) Kessissoglou, D. P.; Kirk, M. L.; Bender, C. A.; Lah, M. S.; Pecoraro, V. L. *J. Chem. Soc., Chem. Commun.* **1989**, 84.
(23) Bonadies, J. A.; Kirk, M. L.; Lah, M. S.; Kessissoglou, D. P.; Hatfield, W. E.; Pecoraro, V. L. *Inorg. Chem.* **1989**, *28*, 2037.

S0020-1669(96)00183-8 CCC: $12.00

binuclear, trinuclear, or polymeric complexes containing μ_2-oxo[28−34] and carboxylato bridges.[35−42]

In this paper we report the synthesis and characterization of mixed-valence $Mn^{III}Mn^{II}Mn^{III}$(*Hsaladhp*)$_2$(AcO)$_2$(*5-X-sal*)$_2$(*thf*)$_2$ compounds, the crystal structures of $Mn^{III}Mn^{II}Mn^{III}$(*5-Cl-Hsaladhp*)$_2$(AcO)$_4$(MeOH)$_2$·4CH_3OH (**1a**), $Mn^{III}Mn^{II}Mn^{III}$(*Hsaladhp*)$_2$(AcO)$_2$(*5-Cl-Sal*)$_2$(*thf*)$_2$ (**3a**) and $Mn^{II}Mn^{II}Mn^{II}$ (AcO)$_6$(*pybim*)$_2$ (**1b**) as well as the behavior in the solid and in solution of these compounds.

Experimental Section

The following abbreviations are used throughout the text: *H$_3$saladhp* = 1,3-dihydroxy-2-methyl(salicylideneamino)propane; *5-Cl-H$_3$saladhp* = 1,3-dihydroxy-2-methyl(5-chlorosalicylideneamino)propane; HOAc = acetic acid; *H$_2$sal* = salicylic acid; *5-Cl-H$_2$sal* = 5-chlorosalicylic acid; *pybim* = 2-(2-pyridyl)benzimidazole; *dmf* = dimethylformamide; *thf* = tetrahydrofuran; *Hcapca* = *N*-[2-(2-pyridylmethyleneamino)-phenyl]pyridine-2-carboxamide.

Materials. The chemicals for the synthesis of the compounds were used as purchased. Acetonitrile (CH_3CN) was distilled from calcium hydride (CaH_2) and CH_3OH from magnesium (Mg), and both were stored over 3 Å molecular sieves. Diethyl ether, anhydrous grade, and absolute ethanol were used without any further purification. Salicylaldehyde, 5-chlorosalicylaldehyde, 2-amino-2-methyl-1,3-propanediol, salicylic acid, 5-chlorosalicylic acid, and Mn(AcO)$_2$·4H_2O were purchased from Aldrich Co. All chemicals and solvents were reagent grade.

Physical Measurements. Infrared spectra (400−4000 cm^{-1}) were recorded on a Perkin-Elmer FT-IR 1650 spectrometer with samples prepared as KBr pellets. UV−vis spectra were recorded on a Shimadzu-160A dual beam spectrophotometer. ESR spectra were recorded on a Bruker ESR 300 spectrometer equipped with a Varian variable temperature controller. *dpph* was used as an external standard. Room temperature magnetic measurements were carried out by Faraday's method using mercury tetrathiocyanatocobaltate(II) as a calibrant. C, H, and N elemental analysis were performed on a Perkin-Elmer 240B elemental analyzer, Mn was determined by atomic absorption spectroscopy on a Perkin-Elmer 1100B spectrophotometer. The magnetic measurements were carried out on a polycrystalline sample (30.0 mg) using a Quantum Design Squid susceptometer, and 65 points were collected in the temperature range 4.00−300 K. The applied magnetic field was 1000.00 G. The correction for the diamagnetism of the complex was estimated from Pascal constants; a value of 56×10^{-6} cm^3 mol^{-1}, was used for the temperature independent paramagnetism (TIP) of the Mn ion. The magnetism of the sample was found to be field independent. Electric conductance measurements were carried out with a WTW Model LF 530 conductivity outfit and a type C cell, which had a cell constant of 0.996. This represents a mean value calibrated at 25 °C with potassium chloride. All temperatures were controlled with an accuracy of ±0.1 °C using a Haake thermoelectric circulating system.

Preparation of the Compounds. The Schiff-bases were synthesized by condensation of salicylaldehyde or 5-chlorosalicylaldehyde with 2-amino-2-methyl-1,3-propanediol.

$Mn^{III}Mn^{II}Mn^{III}$(5-Cl-*Hsaladhp*)$_2$(AcO)$_4$(CH_3OH)$_2$·4CH_3OH (1a). Ten millimoles (1.56 g) of 5-Cl-salicylaldehyde was added to a solution of 10 mmol (1.05 g) of 2-amino-2-methyl-1,3-propandiol in 100 mL of MeOH. The resulting mixture was refluxed for 1 h, generating a pale yellow solution. When the solution was cooled to room temperature, 15 mmol of Mn(acetato)$_2$·4H_2O (3.7 g) was added with stirring. This reaction mixture was refluxed for 1 h, after which the solution was allowed to cool to room temperature and was exposed to dioxygen by bubbling air into the reaction mixture. Green-brown crystals of **1a** were obtained by slow evaporation. The crystalline product was characterized by elemental analysis with the formula $C_{36}H_{60}Cl_2N_2O_{20}Mn_3$ (fw = 1076.58). Yield: 70%. Anal. Calcd: C, 40.1; H, 5.60; N, 2.60; Mn, 15.30. Found: C, 40.3; H, 5.90; N, 2.70; Mn, 15.10. IR (KBr pellet, cm^{-1}): ν(O−H) 3210 (vs), ν(C═N) 1615 (vs), ν_{as}(CO_2) 1590 (vs), ν(C═O) 1540 (s), ν_{sym}(CO_2) 1425 (vs). UV−vis [λ (ϵ, M^{-1} cm^{-1}), CH_2Cl_2]: 463 (1900), 390 (5900), 300 (18850) nm.

$Mn^{III}Mn^{II}Mn^{III}$(*Hsaladhp*)$_2$(AcO)$_2$(*Hsal*)$_2$(*thf*)$_2$ (2a). Ten millimoles (1.1 mL) of salicylaldehyde was added to a solution of 10 mmol (1.05 g) of 2-amino-2-methyl-1,3-propanediol in 100 mL of CH_3OH. The resulting mixture was refluxed for 1 h, generating a pale yellow solution. When the solution was cooled to room temperature, 15 mmol of Mn(AcO)$_2$·4H_2O (3.7 g) was added with stirring. This reaction mixture was refluxed for 1 h, after which the solution was allowed to cool to room temperature and was exposed to dioxygen by bubbling air into the reaction mixture. Green-brown crystals of $Mn^{III}Mn^{II}Mn^{III}$(*Hsaladhp*)$_2$(AcO)$_4$(CH_3OH)$_2$ (**1**) were obtained by slow evaporation. Then 3 mmol of **1** (2.8 g) was dissolved in 10 mL of *thf*. To this black-red solution was added 6 mmol (0.83 g) of salicylic acid dissolved in 50 mL of *thf* and the reaction mixture was refluxed for 1 h. A brown crystalline product was deposited in a few days by slow evaporation. The crystalline product was characterized by elemental analysis with the formula $C_{48}H_{58}N_2O_{18}Mn_3$ (fw = 1115.7). Yield: 70%. Anal. Calcd: C, 51.60; H, 5.20; N, 3.10; Mn, 14.90. Found: C, 51.10; H, 5.50; N, 3.00; Mn, 14.50. IR (KBr pellet, cm^{-1}): ν(O−H) 3210 (vs), ν(C═N) 1615 (vs), ν_{as}(CO_2) of acetate 1590 (vs), ν_{as}(CO_2) of salicylic acid 1580 (vs), ν(C═O) 1540 (s), ν_{sym}(CO_2) of acetate 1425 (vs), ν_{sym}(CO_2) of salicylic acid 1375 (vs). UV−vis [λ (ϵ, M^{-1} cm^{-1}), CH_2Cl_2]: 480 (1650), 380 (4600), 300 (14400) nm.

$Mn^{III}Mn^{II}Mn^{III}$(*Hsaladhp*)$_2$(AcO)$_2$(*5-Cl-Hsal*)$_2$(*thf*)$_2$ (3a). The compound was prepared in a fashion similar to that used for **2a**, except that 5-chlorosalicylic acid was used instead of salicylic acid. Brown/green crystals suitable for X-ray diffraction studies were obtained by slow evaporation. The crystalline product was characterized by elemental analysis with the formula $C_{48}H_{56}Cl_2N_2O_{18}Mn_3$ (fw = 1184.67). Yield: 70%. Anal. Calcd: 48.60; H, 4.70; N, 2.35; Mn, 14.05. Found: C, 48.10; H, 4.60; N, 2.20; Mn, 13.70. IR (KBr pellet, cm^{-1}) ν(O−H) 3300 (s, br) 3210 (vs), ν(C═N) 1615 (vs), ν_{as}(CO_2) of acetate 1586 (vs), ν_{as}(CO_2) of salicylic acid 1578 (vs), ν(C═O) 1540 (s), ν_{sym}(CO_2) of acetate 1432 (vs), ν_{sym}(CO_2) of salicylic acid 1410 (s), ν(C−Cl) 714 (s). UV−vis [λ (ϵ, M^{-1} cm^{-1}), CH_2Cl_2]: 465 (1800), 385 (5300), 290 (17600) nm.

$Mn^{II}Mn^{II}Mn^{II}$(*pybim*)$_2$(AcO)$_6$ (1b). To a suspension of 1.12 mmol (0.300 g) of Mn(AcO)$_3$·2H_2O in 25 mL of methanol was added 1.12 mmol (0.338 g) of *N*-[2-(2-pyridylmethyleneamino)phenyl]pyridine-2-carboxamide. The suspension was refluxed for 2 days. The volume of the resulting deep brown-red solution was reduced to 5 mL, and

(24) Kessissoglou, D. P.; Butler, W. M.; Pecoraro, V. L. *Inorg. Chem.* **1987**, *26*, 495.
(25) Kessissoglou, D. P.; Kirk, M. L.; Lah, M. S.; Li, X.-H.; Raptopoulou, C. A.; Hatfield, W. E.; Pecoraro, V. L. *Inorg. Chem.* **1992**, *31*, 5424.
(26) Malamatari, D. A.; Hitou, P.; Hatzidimitriou, A. G.; Inscore, F. E.; Gourdon, A.; Kirk, M. L.; Kessissoglou, D. P. *Inorg. Chem.* **1995**, *34*, 2493.
(27) Kirk, M. L.; Lah, M. S.; Raptopoulou, C. A.; Kessissoglou, D. P.; Hatfield, W. E.; Pecoraro, V. L. *Inorg. Chem.* **1991**, *30*, 3900.
(28) Larson, E. J.; Lah, M. S.; Li, X.-H.; Bonadies, J. A.; Pecoraro, V. L. *Inorg. Chem.* **1992**, *31*, 373.
(29) Larson, E. J.; Pecoraro, V. L. *J. Am. Chem. Soc.* **1991**, *113*, 3810.
(30) Gelasco, A.; Pecoraro, V. L. *J. Am. Chem. Soc.* **1993**, *115*, 7928.
(31) Larson, E. J.; Riggs, P.; Penner-Hahn, J. E.; Pecoraro, V. L. *J. Chem. Soc., Chem. Commun.* **1992**, 102.
(32) Larson, E. J.; Haddy, A.; Kirk, M. L.; Sands, R.; Hatfield, W. *Pecoraro*, V. L. *J. Am. Chem. Soc.* **1992**, *114*, 6263.
(33) Chan, M. K.; Armstrong, W. H. *J. Am. Chem. Soc.* **1989**, *111*, 9121.
(34) Goodson, P. A.; Glerup, J.; Hodgson, D. J.; Michelsen, K.; Weike, H. *Inorg. Chem.* **1991**, *30*, 4909.
(35) Schake, A. R.; Schmitt, E. A.; Conti, A. J.; Streib, W. E.; Huffman, J. C.; Hendrickson, D. N.; Christou, G. *Inorg. Chem.* **1991**, *30*, 3192.
(36) Shihaba, S.; Onuma, S.; Inoue, H. *Inorg. Chem.* **1985**, *24*, 1723.
(37) Auger, N.; Girerd, J.-J.; Corbella, M.; Gleizes, A.; Zimmerman, J.-L. *J. Am. Chem. Soc.* **1990**, *112*, 448.
(38) Rardin, R. L.; Bino, A.; Poganiuch, P.; Tolman, W. B.; Liu, S.; Lippard, S. J. *Angew. Chem., Int. Ed. Engl.* **1990**, *29*, 812.
(39) Rardin, R. L.; Poganiuch, P.; Bino, A.; Goldberg, D. P.; Tolman, W. B.; Liu, S.; Lippard, S. J. *J. Am. Chem. Soc.* **1992**, *114*, 5240.
(40) Davies, J. E.; Gatehouse, B. M.; Murray, K. S. *J. Chem. Soc., Dalton Trans.* **1973**, 2523.
(41) Murray, B. D.; Hope, H.; Power, P. P. *J. Am. Chem. Soc.* **1985**, *107*, 169.
(42) Aurangzeb, N.; Hulme, C. E.; McAuliffe, C. A.; Pritchard, R. G.; Watkinson, M.; Garcia-Deibe, A.; Bermejo, M. R.; Sousa, A. *J. Chem. Soc., Chem. Commun.* **1992**, 1524.

Table 1. Crystallographic Data for **1a**, **3a**, and **1b**

	1a	**3a**	**1b**
formula	$C_{36}H_{60}O_{20}N_2Cl_2Mn_3$	$C_{48}H_{56}O_{18}N_2Cl_2Mn_3$	$C_{36}H_{36}O_{12}N_6Mn_3$
a, Å	9.272(7)	8.776(3)	13.345(6)
b, Å	11.046(8)	22.182(7)	8.514(4)
c, Å	12.635(9)	13.575(4)	9.494(4)
α, deg	76.78(2)		75.48(1)
β, deg	81.84(2)	94.44(1)	75.83(1)
γ, deg	85.90(2)		76.42(1)
V, Å^3	1246(2)	2635(1)	995.1(8)
Z	1	2	1
fw	1076.58	1184.67	909.53
space group	$P\bar{1}$	$P2_1/n$	$P\bar{1}$
T, °C	23	23	23
λ, Å	0.7107	0.7107	0.7107
ρ_{obsd}, g cm^{-3}	1.42	1.47	1.50
ρ_{calcd}, g cm^{-3}	1.435	1.493	1.518
μ, cm^{-1}	9.28	8.83	10.05
R1	0.0349	0.0378	0.0298
wR2[a]	0.0941	0.0957	0.0758

[a] $w = 1/[\sigma^2(F_o^2) + (aP)^2 + bP]$ and $P_2 = (\max(F_o^2, 0) + 2F_c^2)/3$. $a = 0.0461$, $b = 0.5307$ for **1a**, $a = 0.0375$, $b = 1.7402$ for **3a**, amd $a = 0.0233$, $b = 0.4210$ for **1b**. $R1 = \sum(|F_o - F_c|)/\sum(|F_o|)$. $wR2 = \{\sum[w(F_o^2 - F^{c2})^2]/\sum[w(F_o^2)^2]\}^{1/2}$ for reflections with $I > 2\sigma(I)$.

diethyl ether (30 mL) was added dropwise under stirring. The brown-red precipitate was filtered off, washed with diethyl ether, and dried under vacuum. Orange-red crystals suitable for X-ray diffraction studies were obtained by slow evaporation of a methanol solution of the complex. Yield: 0.21 g (41%) based on manganese. The crystalline product was characterized by elemental analysis with the formula $C_{36}H_{36}N_6O_{12}Mn_3$ (fw = 909.53). Anal. Calcd: C, 47.55; H, 4.00; N, 9.25; Mn, 18.10. Found: C, 47.30; H, 4.20; N, 9.00; Mn, 18.40. IR (KBr pellet, cm^{-1}): $\nu_{as}(CO_2)$ 1575 (vs, br), $\nu_{sym}(CO_2)$ 1415 (vs, br). UV−vis[λ (ϵ, M^{-1} cm^{-1}), MeOH]: 520 sh (1200), 340 sh (15200), 320 (63200), 308 (70600), 243 sh (40400) nm.

X-ray Crystal Structure Determination. A green-brown prismatic crystal of **3a** with approximate dimensions 0.12 × 0.22 × 0.50 mm and an orange crystal of **1b** with approximate dimensions 0.20 × 0.20 × 0.40 mm were mounted in air, while a green-brown prismatic crystal of **1a** with approximate dimensions 0.15 × 0.15 × 0.50 was mounted in capillary filled with drops of mother liquid. Diffraction measurements were made on a Crystal Logic dual goniometer diffractometer using graphite-monochromated Mo radiation. Crystal data and parameters for data collection are reported in Table 1. Unit cell dimensions were determined and refined by using the angular settings of 25 automatically centered reflections in the range $11° < 2\theta < 23°$. Intensity data were recorded using $\theta-2\theta$ scan to $2\theta(\max) = 50°$ with scan speed 3.3 deg/min for **1a**, 1.8 deg/min for **3a** and 2.0 deg/min for **1b** and scan range 2.5° plus $\alpha_1\alpha_2$ separation. Three standard reflections monitored every 97 reflections, showed <3.0% intensity fluctuation and no decay. Lorentz, polarization, and ψ-scan absorption corrections were applied using Crystal Logic software.

Symmetry equivalent data of **1a**, **3a**, and **1b** were averaged with $R(\text{int}) = 0.0149$, 0.0327, and 0.0104 respectively to give 4380, 4652, and 3503 independent reflections from a total of 4622, 5188, and 3761 collected while 4377, 4649, and 3498 reflections were used in the refinement, due to large negative F^2 values or because they were at very low 2θ values and affected by the beam stop. The structures were solved by direct methods using the programs SHELXS-86[43] and refined by full-matrix least-squares techniques on F^2 with SHELXL-93[44] using 4377 reflections for **1a**, 4649 reflections for **3a**, and 3498 reflections for **1b** and refining 397, 429, and 331 parameters respectivity. All hydrogen atoms [except those of the methyl group of one of the methanol solvent molecules for **1a** and those of C(22) and C(23) for **3a** which were introduced at calculated positions as riding on bonded atoms] were located by difference maps and their positions were refined isotropically. All non-hydrogen atoms were refined anisotropically.

(43) Sheldrick, G. M., SHELX 86, University of Goettingen, Germany, 1986.
(44) Sheldrick, G. M., SHELX 93: Crystal Structure Refinement, University of Goettingen, Germany, 1993.

Table 2. Positional Parameters (×10^4) and Equivalent Thermal Parameters (Å^2 × 10^3) of the Non-H Atoms of **1a**[a]

	x	*y*	*z*	U_{eq}
Mn(1)	5000	5000	5000	43(1)
Mn(2)	4024(1)	7605(1)	3022(1)	41(1)
N	2098(2)	8285(2)	3634(2)	42(1)
O(1)	4308(2)	9098(1)	1955(1)	52(1)
O(2)	3456(2)	6155(1)	4067(1)	45(1)
O(3)	1373(2)	8825(2)	5766(2)	70(1)
O(4)	5887(2)	6980(2)	2347(1)	57(1)
O(5)	3349(2)	4605(2)	6388(1)	61(1)
O(6)	5321(2)	8223(1)	4154(1)	50(1)
O(7)	4364(2)	3393(1)	4457(1)	56(1)
O(8)	2932(4)	6746(2)	1865(2)	94(1)
C(1)	3466(2)	10119(2)	1739(2)	43(1)
C(2)	3901(3)	11055(2)	815(2)	53(1)
C(3)	3083(3)	12155(2)	563(2)	59(1)
C(4)	1808(3)	12344(2)	1234(2)	55(1)
C(5)	1330(3)	11450(2)	2125(2)	50(1)
C(6)	2139(2)	10315(2)	2391(2)	42(1)
C(7)	1529(2)	9381(2)	3309(2)	44(1)
C(8)	1334(2)	7388(2)	4590(2)	49(1)
C(9)	1918(3)	6119(2)	4385(2)	52(1)
C(10)	1800(3)	7596(2)	5643(2)	53(1)
C(11)	−326(3)	7494(3)	4632(3)	71(1)
C(12)	6846(3)	6182(2)	2744(2)	52(1)
C(13)	8327(4)	6221(5)	2073(3)	86(1)
C(14)	5668(2)	7746(2)	5093(2)	43(1)
C(15)	6117(4)	8599(3)	5752(3)	58(1)
C(16)	2435(7)	7191(5)	886(4)	94(1)
Cl	795(1)	13750(1)	930(1)	87(1)
OM1	6031(4)	5653(2)	7729(3)	107(1)
CM1	4743(11)	6002(6)	8324(5)	136(3)
OM2	2755(4)	9925(3)	7041(3)	114(1)
CM2	2316(5)	9904(5)	8131(4)	118(2)

[a] Esd's in parentheses. $U_{eq} = {}^1/_3(U_{11} + U_{22} + U_{33})$.

The final values for R_1, wR2, and GOF, for observed data with $I > 2\sigma(I)$ are given in Supporting Information and for all data are 0.0413, 0.1004, and 1.038 (**1a**), 0.0597, 0.1104, and 1.040 (**3a**) and, 0.0382, 0.0832, and 1.061 (**1b**), respectively. The maximum and minimum residual peaks in the final difference map were +0.439 and −0.380 e/Å^3 for **1a**, +0.376 and −0.306 e/Å^3 for **3a**, and +0.303 and −0.320 e/Å^3 for **1b**. The largest shifts/esd in the final cycle were 0.033, 0.035, and 0.037 respectively. Positional and *U*(equiv) thermal parameters are given in Tables 2−4.

Results and Discussion

Synthesis. The mixed-valence compounds can be prepared in two steps. By addition of the Schiff-base ligand to $Mn(AcO)_2{\cdot}4H_2O$ or $Mn(AcO)_3$ in methanol and exposure to air the trinuclear complexes of the general composition $Mn^{III}Mn^{II}Mn^{III}(X\text{-}\textit{Hsaladhp})_2(AcO)_4(CH_3OH)_2$ are isolated.[6] These trimers react with X-salicylic acid in methanol, *dmf*, or *thf* to yield mixed acetato/salicylato trinuclear complexes which are isolated as dark brown solids. The reaction can take place in all three solvents leading to the formation of trinuclear compounds in contrast to the preparation of the trinuclear complexes with only acetates as bridging ligands for which in the presence of *dmf*, mononuclear Mn^{IV} complexes[19,20] and MnO_2 are formed exclusively. To obtain the trinuclear compounds it is absolutely essential not to add additional strong bases such as sodium methoxide or sodium hydroxide which lead to mononuclear Mn^{IV} complexes. We should mention that in the presence of CH_3CN a polymeric compound with the same trimeric unit $[Mn^{III}Mn^{II}Mn^{III}]$ but with significant deviation from linearity, $Mn^{III}-Mn^{II}-Mn^{III} = 137.5°$, has previously been isolated and structurally characterized.[26] Generally nitrogen-donor solvents e.g. CH_3CN, *py*, and *en* are not bound at the sixth position of

Table 3. Positional Parameters ($\times 10^4$) and Equivalent Thermal Parameters (Å^2 $\times$ 10^3) of the Non-H Atoms of **3a**[a]

	x	*y*	*z*	U_{eq}
Mn(1)	0	5000	10000	35(1)
Mn(2)	1207(1)	6177(1)	8521(1)	40(1)
O(1)	1837(3)	6975(1)	8351(2)	56(2)
O(2)	795(2)	5352(1)	9655(1)	40(1)
O(3)	5627(3)	5318(1)	8431(3)	83(2)
O(4)	−715(3)	6467(1)	8980(2)	55(2)
O(5)	−1468(3)	5783(1)	10035(2)	57(2)
O(6)	2374(3)	6259(1)	9986(2)	53(2)
O(7)	−1830(3)	4541(1)	9115(2)	56(2)
O(8)	3491(4)	7216(1)	10805(2)	79(3)
O(9)	−258(3)	6163(1)	6948(2)	61(1)
N(1)	2884(3)	5876(1)	7745(2)	38(1)
C(1)	2818(4)	7201(1)	7761(3)	51(2)
C(2)	2933(6)	7839(2)	7688(4)	74(3)
C(3)	3889(7)	8085(2)	7055(4)	88(4)
C(4)	4752(6)	7743(2)	6458(4)	81(3)
C(5)	4699(5)	7136(2)	6547(3)	66(2)
C(6)	3753(4)	6852(2)	7197(3)	49(2)
C(7)	3777(4)	6206(2)	7251(2)	44(2)
C(8)	3047(4)	5205(1)	7760(2)	40(2)
C(9)	1453(4)	4984(1)	7949(2)	43(2)
C(10)	4204(4)	5045(2)	8620(3)	52(2)
C(11)	3528(5)	4943(2)	6792(3)	58(3)
C(12)	−1671(4)	6251(1)	9538(2)	46(2)
C(13)	−3117(6)	6607(2)	9611(5)	72(3)
C(14)	2344(4)	5986(1)	10800(2)	42(2)
C(15)	2962(4)	6307(1)	11704(2)	43(2)
C(16)	2957(4)	6022(2)	12165(2)	50(2)
C(17)	3473(5)	6323(2)	13460(3)	63(2)
C(18)	3931(6)	6921(2)	13427(3)	80(4)
C(19)	3934(6)	7206(2)	12534(4)	78(3)
C(20)	3472(4)	6906(2)	11662(3)	57(2)
C(21)	117(6)	6350(3)	5997(3)	75(3)
C(22)	−1142(8)	6146(4)	5289(5)	141(6)
C(23)	−2120(7)	5756(4)	5829(4)	121(4)
C(24)	−1774(5)	5922(3)	6880(4)	84(3)
Cl(1)	3539(2)	5946(1)	14590(1)	94(1)

[a] Esd's in parentheses. $U_{eq} = {}^1/_3(U_{11} + U_{22} + U_{33})$.

the Mn^{III} ion. The reactions involve deprotonation of the ligand without using a base, e.g.

$$XC_6H_3(OH)CHO + H_2NC(R)(CH_2OH)_2 \xrightarrow{MeOH} XC_6H_3(O)CH{=}NC(R)(CH_2OH)_2$$

$$XC_6H_3(O)CH{=}NC(R)(CH_2OH)_2 + Mn(AcO)_2{\cdot}4H_2O \xrightarrow{MeOH} Mn^{III}Mn^{II}Mn^{III}[XC_6H_3(O)CH{=}NC(R)(CH_2O)(CH_2OH)]_2(AcO)_4(CH_3OH)_2$$

$$Mn^{III}Mn^{II}Mn^{III}[(XC_6H_3(O)CH{=}NC(R)(CH_2O)(CH_2OH)]_2(AcO)_4(CH_3OH)_2 + X\text{-}H_2Sal \xrightarrow{thf} Mn^{III}Mn^{II}Mn^{III}[(XC_6H_3(O)CH{=}NC(R)(CH_2O)(CH_2OH)]_2(AcO)_2(X\text{-}Hsal)_2(thf)$$

The mixed valence trinuclear compounds are green-brown crystalline solids that appear to be air and moisture stable. They are soluble in *dmso*, *dmf*, CH_2Cl_2, *thf*, and $CHCl_3$ but are insoluble in water. The behavior of the complexes as electrolytes shows a different degree of dissociation in various solvents leading to the general conclusion that in CH_2Cl_2 and *thf* no dissociation occurs while in *dmf*, and *dmso* partial dissociation is observed.

The $Mn^{II}Mn^{II}Mn^{II}$ complex can be obtained from the reaction of $Mn(AcO)_2$ or $Mn(AcO)_3$ with *Hcapca*, in CH_3OH (Scheme 1). The formation of the bidentate, nitrogen-donating ligand can be achieved only with reflux of the reaction mixture, while at room temperature $MnCl_2$ results in the formation of the mononuclear Mn^{III}(*Hcapca*)$(py)_2$.[45]

Table 4. Positional Parameters ($\times 10^4$) and Equivalent Thermal Parameters (Å^2 $\times$ 10^3) of the Non-H Atoms of **1b**[a]

	x	*y*	*z*	U_{eq}
Mn(1)	5000	0	0	37(1)
Mn(2)	7044(1)	−2828(1)	1601(1)	39(1)
O(1)	5385(1)	726(2)	1795(2)	57(1)
O(2)	6763(1)	−865(2)	2680(2)	61(1)
O(3)	4481(1)	−2150(2)	1505(2)	58(1)
O(4)	5700(1)	−3785(2)	2702(2)	59(1)
O(5)	8335(1)	−1901(2)	−1191(2)	55(1)
O(6)	6627(1)	−1466(2)	−452(2)	47(1)
N(1)	7676(1)	−5365(2)	846(2)	42(1)
N(2)	8579(1)	−3839(2)	2241(2)	39(1)
N(3)	10055(1)	−5738(2)	2218(2)	39(1)
C(1)	7177(2)	−6105(3)	218(3)	51(1)
C(2)	7582(2)	−7646(3)	−125(3)	54(1)
C(3)	8533(2)	−8466(3)	212(3)	56(1)
C(4)	9068(2)	−7720(3)	863(3)	49(1)
C(5)	8613(2)	−6171(3)	1165(2)	37(1)
C(6)	9088(2)	−5264(2)	1874(2)	35(1)
C(7)	9270(2)	−3334(3)	2847(2)	39(1)
C(8)	10198(2)	−4518(3)	2844(2)	39(1)
C(9)	11031(2)	−4362(4)	3407(3)	52(1)
C(10)	10904(2)	−2960(4)	3940(3)	64(1)
C(11)	9990(2)	−1753(4)	3916(4)	66(1)
C(12)	9154(2)	−1915(3)	3387(3)	53(1)
C(21)	6024(2)	367(3)	2634(3)	45(1)
C(22)	5932(4)	1495(4)	3671(4)	73(1)
C(23)	4777(2)	−3326(3)	2483(3)	46(1)
C(24)	3973(3)	−4287(5)	3497(5)	78(1)
C(25)	7443(2)	−1420(3)	−1481(2)	41(1)
C(26)	7295(3)	−789(6)	−3042(3)	74(1)

[a] Esd's in parentheses. $U_{eq} = {}^1/_3(U_{11} + U_{22} + U_{33})$.

Scheme 1. Pathways for the Formation of Compound **1b**

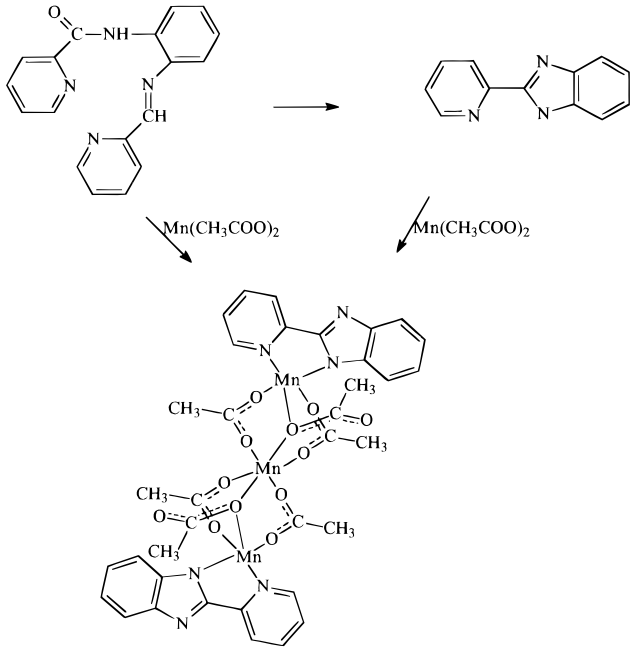

Description of the Structure of 1a. ORTEP diagram of complex **1a** is shown as Figure 1. Bond distances and angles for the coordination spheres are listed in Table 5. The complex includes a central octahedral Mn^{II} ion, Mn(1), located on a crystallographic inversion center. It is flanked to two tetrago-

(45) Soulti, K.; Malamatari, D. A.; Raptopoulou, C. P.; Terzis, A.; Kabanos, T. A.; Kessissoglou, D. P. Manuscript in preparation.

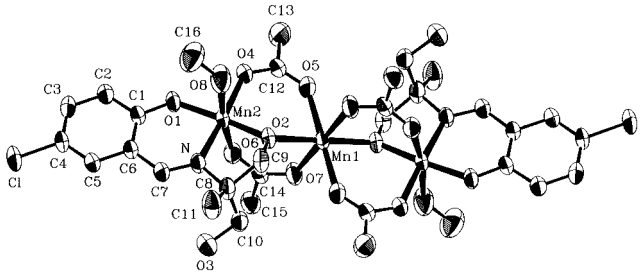

Figure 1. ORTEP view of **1a** with 50% thermal ellipsoids showing the atom labeling scheme.

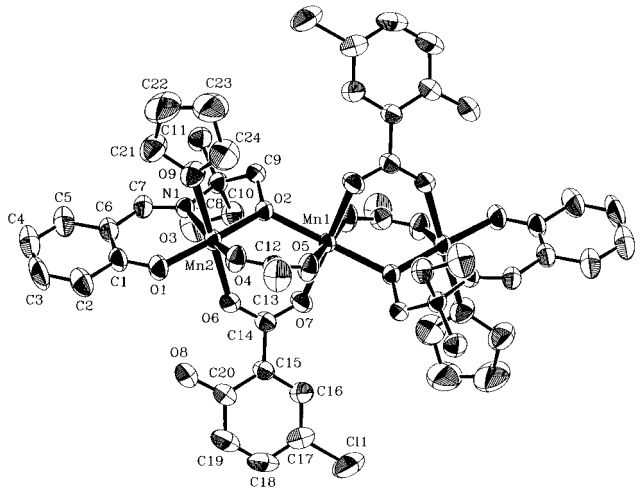

Figure 2. ORTEP view of **3a** with 50% thermal ellipsoids showing the atom labeling scheme.

Table 5. Selected Bond Distances (Å) and Angles (deg) of **1a**

Bond Distances			
Mn(1)···Mn(2)	3.511	Mn(2)−O(2)	1.882(2)
Mn(1)−O(2)	2.144(2)	Mn(2)−N	2.007(2)
Mn(1)−O(5)	2.143(2)	Mn(2)−O(6)	2.238(2)
Mn(1)−O(7)	2.189(2)	Mn(2)−O(8)	2.291(3)
Mn(2)−O(1)	1.884(2)	Mn(2)−O(4)	1.966(2)
Bond Angles			
O(2)−Mn(1)−O(5)	89.99(8)	O(2)−Mn(2)−O(6)	92.73(8)
O(2)−Mn(1)−O(7)	89.59(7)	O(4)−Mn(2)−O(6)	86.62(9)
O(5)−Mn(1)−O(7)	89.44(8)	O(6)−Mn(2)−N	95.33(8)
O(1)−Mn(2)−O(2)	171.87(7)	O(1)−Mn(2)−O(8)	91.59(10)
O(1)−Mn(2)−O(4)	87.13(8)	O(2)−Mn(2)−O(8)	84.10(10)
O(2)−Mn(2)−O(4)	99.45(8)	O(4)−Mn(2)−O(8)	86.62(11)
O(1)−Mn(2)−N	90.63(8)	O(8)−Mn(2)−N	91.59(11)
O(2)−Mn(2)−N	82.64(8)	O(6)−Mn(2)−O(8)	171.96(8)
O(4)−Mn(2)−N	177.09(7)	Mn(2)−O(2)−Mn(1)	121.27(9)
O(1)−Mn(2)−O(6)	92.42(9)		

nally distorted Mn^{III} ions Mn(2). The coordination octahedral environment of central Mn^{II} is composed of four bridging acetates and two μ-alkoxo oxygen atoms of the Schiff base ligand. Each Mn^{III} is six coordinate using two acetates, a tridentate Schiff base ligand, and a methanol molecule. The bond distances and angles are very similar with those reported previously.[21] The Mn···Mn separation is 3.511 Å. More detail analysis of the coordination environment of the manganese atoms is given in the following description of **3a**.

Description of the Structure of 3a. An ORTEP diagram of complex **3a** is shown as Figure 2. Bond distances and angles for the coordination spheres are listed in Table 6. The complex includes a central octahedral Mn^{II} ion, Mn(1), located on a crystallographic inversion center. It is flanked by two tetragonally distorted Mn^{III} ions Mn(2). The coordination octahedral environment of central Mn^{II} is composed of two *syn*-bridging acetates and salicylates and two μ-alkoxo oxygen atoms of the

Table 6. Selected Bond Distances (Å) and Angles (deg) of **3a**

Bond Distances			
Mn(1)···Mn(2)	3.507	Mn(2)−O(2)	1.877(2)
Mn(1)−O(2)	2.151(2)	Mn(2)−N(1)	1.991(3)
Mn(1)−O(5)	2.166(2)	Mn(2)−O(6)	2.174(3)
Mn(1)−O(7)	2.182(2)	Mn(2)−O(9)	2.405(3)
Mn(2)−O(1)	1.873(2)	Mn(2)−O(4)	1.951(3)
Bond Angles			
O(2)−Mn(1)−O(5)	87.72(9)	O(2)−Mn(2)−O(6)	94.20(9)
O(2)−Mn(1)−O(7)	88.59(9)	O(4)−Mn(2)−O(6)	92.16(11)
O(5)−Mn(1)−O(7)	88.46(10)	N(1)−Mn(2)−O(6)	101.33(10)
O(1)−Mn(2)−O(2)	173.60(10)	O(1)−Mn(2)−O(9)	92.61(10)
O(1)−Mn(2)−O(4)	89.93(11)	O(2)−Mn(2)−O(9)	88.88(9)
O(2)−Mn(2)−O(4)	96.44(10)	O(4)−Mn(2)−O(9)	82.66(10)
O(1)−Mn(2)−N(1)	90.83(11)	N(1)−Mn(2)−O(9)	83.84(10)
O(2)−Mn(2)−N(1)	83.13(10)	O(6)−Mn(2)−O(9)	174.25(9)
O(4)−Mn(2)−N(1)	166.50(10)	Mn(2)−O(2)−Mn(1)	120.95(10)
O(1)−Mn(2)−O(6)	84.86(10)		

Schiff base ligand. Each Mn^{III} is six coordinate using an acetate, a salicylate, a tridentate Schiff base ligand, and a neutral axial oxygen-donor ligand. The neutral unidentate ligand occupies the Jahn−Teller distorted axes along with the salicylato oxygen [O(9) and O(6)] (Figure 2). The elongation is shown by a comparison of Mn(2)−N(1) = 1.991(3) Å and Mn(2)−O(4) = 1.951(3) Å, the longest distances on the equatorial plane, with axial distances Mn(2)−O(6) = 2.174(3) Å and Mn(2)−O(9) = 2.405(3) Å. The *saladhp* ligand acts as a tridentate chelating agent by using an imine nitrogen, and phenolate and alkoxide oxygen atoms to coordinate to Mn^{III}. The equatorial preference has been reported for other mono-, di-, and trinuclear manganese complexes with this and related ligands.[19−26] The Mn^{III}−alkoxide oxygen distance [Mn(2)−O(2) = 1.877(2) Å] is equivalent to the Mn^{III}−phenolate oxygen distance [Mn(2)−O(1) = 1.873(2) Å] even though the former bridges to the Mn^{II} ion. The Mn(III)−alkoxide oxygen distance is also very similar to Mn^{IV}−alkoxide oxygen bonds reported for Mn^{IV}(*saladhp*)$_2$, $Mn-O_{av}$ = 1.889 Å,[19,20] and $[Mn^{IV}(hib)_3]^{2-}$, $Mn-O_{av}$ = 1.841 Å.[46] The central Mn(1) and the terminal Mn(2) ions are bridged by the alkoxide oxygen from the *saladhp* ligand, an acetato, and a carboxylato oxygen from the 5-Cl-salicylato ligand resulting in a 3.507(1) Å Mn(1)···Mn(2) separation with a 120.95(10)° Mn(1)−O(alkoxide)−Mn(2) angle. The acetato oxygen lies on the equatorial plane[47] with a distance of Mn(2)−O(4) = 1.951(3) Å while the salicylato oxygen occupies the axial position of the octahedron with a distance of Mn(2)−O(6) = 2.174(3) Å. The Mn^{III} ions are displaced slightly out of the best least-squares plane defined by O(1), N(1), O(2), and O(4) toward the bridging salicylate moiety by 0.103 Å. This out of plane displacement is also observed for the acetato-only trinuclear analog.[25] The carboxylato atoms of the salicylato ligand [O(6), O(7), C(14)] and the Mn(1) and Mn(2) atoms define a plane with 0.011, 0.064, 0.05, −0.105, and −0.022 Å deviations from planarity respectively, while the phenyl plane is twisted by 23.3° from the O(6)−C(14)−O(7) plane. The *thf* molecules have the envelope form with C(23) 0.356 Å above the C(21)−C(22)−C(24)−O(9) plane. Despite both the bridging ligands being *syn* bound to metal ions, we can distinguish symmetrical and unsymmetrical coordination modes. By comparison of the Mn−O and C−O distances for the acetato and salicylato ligands, it is seen that the coordination mode of the acetato ligands to Mn^{II} and Mn^{III} is unsymmetrical, while that of the salicylato ligands is symmetrical (Scheme 2).

(46) Saadeh, S. M.; Lah, M. S.; Pecoraro, V. L. *Inorg. Chem.* **1991**, *30*, 9.
(47) Pecoraro, V. L. *Manganese Redox Enzymes*; VCH Publishers Inc.: New York, 1992; p 207.

Scheme 2. Coordination Modes of Acetate and Salicylate Ligands

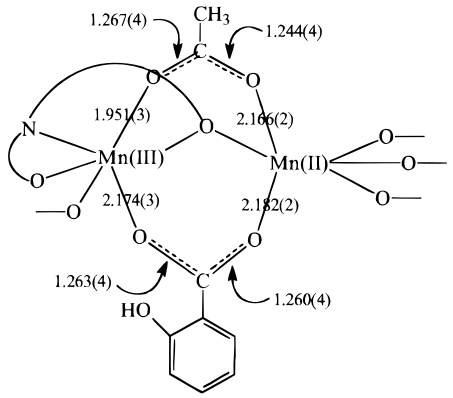

Scheme 3. Inter and Intra H-Bond Network of **3a**

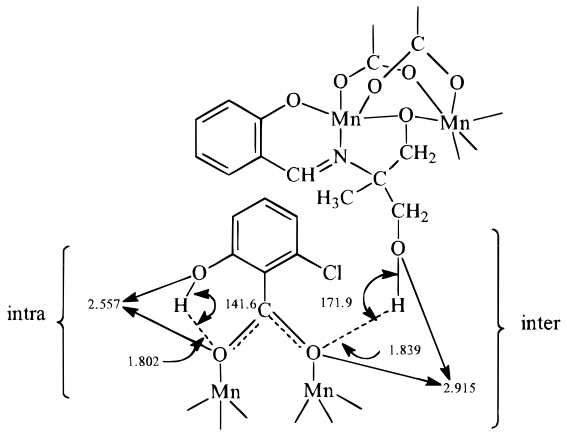

The cluster is valence trapped as evidenced by the long central Mn^{II} to heteroatom bond lengths and by Jahn−Teller distortion of the terminal high spin Mn^{III} ions. The present compound allows the certain assignment of the oxidation state for Mn(1) as a Mn^{II} and for Mn(2) as Mn^{III} ions, while in the starting trinuclear compound for which the sixth position on the terminal manganese atom is occupied by a methanol or water molecule, the question could arise for a deprotonated rather than a protonated form of the ligand.

The molecule shows intra- and inter-hydrogen-bond contacts through phenol hydrogen [HO(8)] and carboxylato oxygen [O(6)] (intra) and alcohol hydrogen [HO(3)] and carboxylato oxygen [O(7)] (inter) (Scheme 3).

Description of the Structure of 1b. Complex **1b** consists of a linear array of divalent manganese ions. An ORTEP diagram of complex **1b** is shown as Figure 3. Bond distances and angles for the coordination spheres are listed in Table 7. The central Mn^{II}, which is located on a crystallographic inversion center, is coordinated octahedrally by six acetate oxygen atoms. The central Mn^{II} and the terminal Mn^{II} atoms are bridged by four acetate ligands in a bidentate fashion, whereas the other two acetate groups form bridges in the monodentate mode.[48−54a] The two terminal Mn^{II} ions are five coordinated with the 2-(2-pyridyl)benzimidazole molecule acting as a bidentate capping ligand.

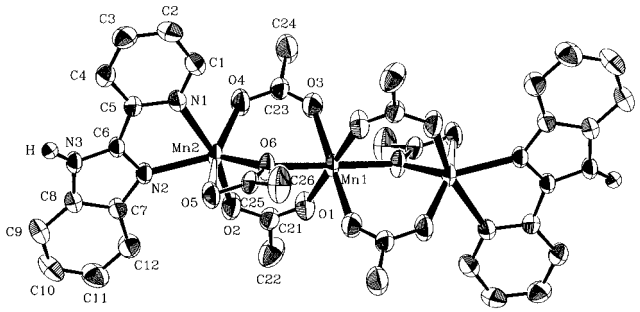

Figure 3. ORTEP view of **1b** with 50% thermal ellipsoids showing the atom labeling scheme.

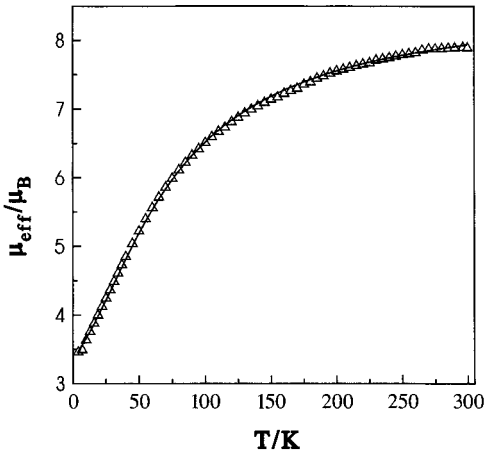

Figure 4. Magnetic susceptibility of **3a** plotted as μ_{eff}/3Mn vs T with the fit to eq 6 (solid line).

Table 7. Selected Bond Distances (Å) and Angles (deg) of **1b**

Bond Distances			
Mn(1)···Mn(2)	3.558	Mn(2)−O(2)	2.088(2)
Mn(1)−O(1)	2.158(2)	Mn(2)−O(6)	2.132(2)
Mn(1)−O(3)	2.162(2)	Mn(2)−N(1)	2.349(2)
Mn(1)−O(6)	2.235(2)	Mn(2)−N(2)	2.197(2)
Mn(2)−O(4)	2.078(2)	Mn(2)···O(5)	2.823
Bond Angles			
O(1)−Mn(1)−O(3)	90.54(8)	O(6)−Mn(2)−N(2)	131.69(6)
O(1)−Mn(1)−O(6)	89.63(7)	O(2)−Mn(2)−N(1)	164.17(7)
O(3)−Mn(1)−O(6)	89.79(7)	O(4)−Mn(2)−N(1)	85.78(8)
O(4)−Mn(2)−O(2)	97.51(8)	N(1)−Mn(2)−O(6)	95.99(7)
O(4)−Mn(2)−O(6)	102.38(7)	N(1)−Mn(2)−N(2)	72.72(6)
O(2)−Mn(2)−O(6)	98.39(8)	O(5)−Mn(2)−O(4)	145.1
O(4)−Mn(2)−N(2)	122.61(7)	Mn(2)−O(6)−Mn(1)	109.08(7)
O(2)−Mn(2)−N(2)	92.68(7)		

The free oxygen atoms of the monodentate acetates interact weakly with the terminal Mn(II) atoms [O(5)···Mn(2) = 2.823, Å] and block the sixth coordination site of the terminal metal ion. The coordination geometry around Mn^{II} is square-pyramidal with severe trigonal distortion as indicated by the trigonallity index[54b] $\tau = (164.17 - 131.69)/60 = 0.54$. The Mn(2) atom is displaced 0.483 Å from the mean basal plane O(2)−O(6)−N(1)−N(2) toward the apical O(4). The O(5)···Mn(2) distance of 2.823 Å is the longest for a series of analogous compounds, and the Mn(2)−O(6) distance of 2.132(2) Å is the shortest obeying the "carboxylate shift" model described by Lippard et al.[39] The metrical parameters for this compound as well as those with similar structure[38,39] reveal that the tricarboxylate-bridged unit can accommodate a considerable

(48) Mehrotra, R. C.; Bohra, R. *Metal Carboxylates*; Academic: New York, 1983.
(49) Cotton, F. A.; Diebold, M. P.; Matusz, M.; Roth, W. J. *Inorg. Chim. Acta* **1986**, *112*, 147.
(50) Prout, K.; Carruthers, J. R.; Rossotti, F. J. C. *J. Chem. Soc. A* **1971**, 3350.
(51) Catterick, J.; Thornton, P. *J. Chem. Soc., Dalton Trans.* **1976**, 1634.
(52) Clegg, W.; Little, I. R.; Straughan, B. P. *J. Chem. Soc., Dalton Trans.* **1986**, 1283.
(53) Clegg, W.; Little, I. R.; Straughan, B. P. *J. Chem. Soc., Chem. Commun.* **1985**, 73.
(54) (a) Clegg, W.; Little, I. R.; Straughan, B. P. *Inorg. Chem.* **1988**, *27*, 1916. (b) Addison, A. W.; Nageswara, T.; Reedijk, J.; van Rijn, J.; Verchoor, G. C. *J. Chem. Soc., Dalton Trans.* **1984**, 1349.

degree of flexibility for Mn···Mn distances (3.37−3.71 Å) something which is not obvious for mixed valence $Mn^{III}Mn^{II}$-Mn^{III} complexes in which the range is much smaller (3.41−3.58 Å).[21,25,26] We mention the existence of a strong hydrogen bond N(3)−H···O(5) ($2 - x, -1 - y, -z$) (N(3)···O(5) = 2.745(2) Å, N(3)−H−O(5) = 171(2)°).

Magnetic Properties of 3a. The molar magnetic susceptibility of **3a** was measured as a function of temperature. The results are shown in Figure 4 in the form of μ_{eff}/3Mn vs T. The value of μ_{eff} decreases from 7.94 μ_B at 300 K to 3.4 μ_B at 4 K. The μ_{eff}/3 Mn value at room temperature, which is comparable with previously reported[25,55] values for $Mn^{III}Mn^{II}Mn^{III}(L)_2(\mu\text{-AcO})_4$-(ROH) (L = tridentate ligand; R = H, CH_3) shows that there is a small antiferromagnetic interaction between the manganese atoms (spin-only value of 2 Mn^{III} and a Mn^{II} is 9.1 μ_B).

By virtue of crystallographic criteria the isotropic Heissenberg Hamiltonian for the complex **3a** is given by eq 1 (**3a** having an

$$H = -2J_1(S_1 \cdot S_2 + S_2 \cdot S_3) - 2J_2(S_1 \cdot S_3) \quad (1)$$

arrangement $S_1 - S_2 - S_3$) where $S_1 = S_3 = 2$ and $S_2 = {}^5/_2$. Because of the large distance between the terminal Mn^{III} ions (7.014 Å) we can exclude this interaction, and therefore the major exchange interaction is expected between the terminal Mn^{III} and the central Mn^{II}. The exchange energies may be calculated by Kambe's method, and are given by

$$E(S,S_{13}) = -J_1[S_T(S_T + 1) - S_{13}(S_{13} + 1) - S_2(S_2 + 1)] \quad (2)$$

For similar compounds, other authors[25] have assumed different g values for Mn^{III} and Mn^{II} in the Zeeman Hamiltonian and have added first- and second-order contributions to the Van Vleck equation. However the use of isotropic g values in the Zeeman term, dealing with the problem of mixed valence polynuclear systems, also gives satisfactory magnetic models. Recently an analogous approach, concerning the isotropic g values, was used in the magnetic study of a mixed-valence Mn^{III}-$Mn^{II}Mn^{III}$ linear chain.[26] Assuming isotropic g values the Zeeman term was added to the preceding Hamiltonian

$$H_{ZEEMAN} = g\mu_B(S_1 + S_2 + S_3)B \quad (3)$$

Because of the extended hydrogen network (see text) a mean field correction was added and the final expression of the susceptibility is given by

$$\chi_{MFC} = \frac{\chi_M}{1 - \dfrac{2zJ\chi_M}{N\mu_B{}^2 g^2}} \quad (4)$$

where χ_M is

$$\chi_M = (Ng^2\mu_B{}^2/3\kappa T)\frac{[\sum_i S_i(S_i + 1)(2S_i + 1)\exp(-E_i/\kappa T)]}{[\sum_i (2S_i + 1)\exp(-E_i/\kappa T)]} \quad (5)$$

The magnetic parameters obtained from the fitting procedure are $J_1 = -5.6$ cm^{-1}, $g = 1.95$, $zJ = -0.25$ cm^{-1}, and $R = 0.003$ where

$$R = \sum_n [(\mu_{eff})_{exptl} - (\mu_{eff})_{calcd}]^2 \quad (6)$$

(55) Baldwin, M. J.; Kampf, J. W.; Kirk, M. L.; Pecoraro, V. L. *Inorg. Chem.* **1995**, *34*, 5255.

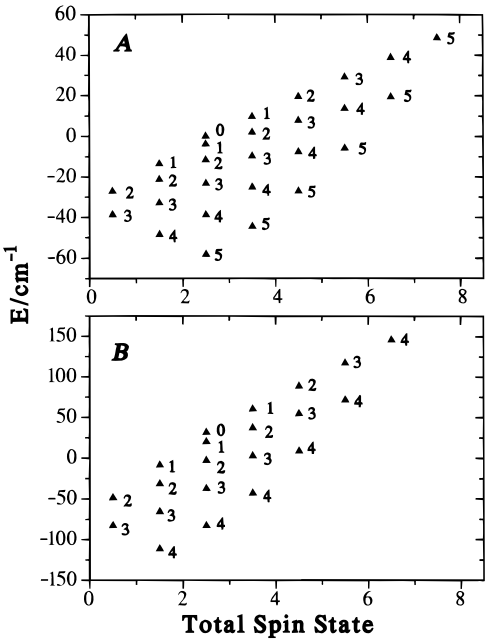

Figure 5. (A) Spin levels for **1b**. (B) Spin levels for **3a**. The energy in cm^{-1} is given as a function of the spin value. To the right of the levels, the S_{13} values are given.

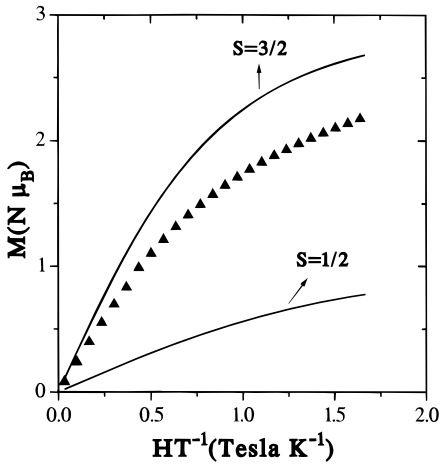

Figure 6. Magnetization study for **3a** at 4 K over the field range 0−5 T as a function of B/T. The solid lines represent the theoretical curves for $S = {}^3/_2$ and $S = {}^1/_2$ states.

Energy levels are represented in Figure 5B with the addition of the S_{13} label. The ground state is found to be the

$$|S_2 = {}^5/_2, S_{13} = 4, S = {}^3/_2\rangle$$

The energy scheme obtained from the susceptibility data is further verified by the isothermal magnetization measurements at 4 K and up to 5 T. The data are given in Figure 6. The two solid lines represent the theoretical magnetization behavior of $S = {}^3/_2$, $S = {}^1/_2$ states and are calculated from the expression

$$M = Ng\mu_B S \cdot B_s(\chi) \quad (7)$$

where $B_s(\chi)$ is the Brillouin function for states with $S = {}^3/_2$ and $S = {}^1/_2$. This clearly shows that the lowest lying state was the $S = {}^3/_2$ with reasonable population of a state, or states, of lower spin.[25]

Magnetic Properties of 1b. The molar magnetic susceptibility of compound **1b** as well as the μ_{eff}/3Mn vs T is shown in Figure 7. Examination of the temperature dependence of the

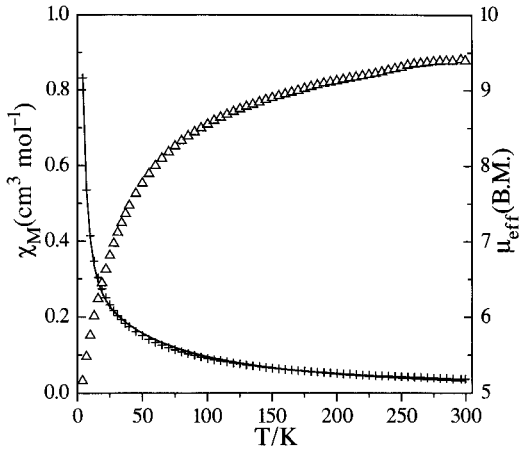

Figure 7. Magnetic susceptibility of **1b** plotted as χ_M vs T (left axis) and μ_{eff}/3Mn vs T (right axis) with the fit to eq 6 (solid line).

μ_{eff}/3Mn reveals that at room temperature its value is 9.4 μ_B and decreases to a value of 5.16 μ_B at 4 K. This decrease from a value of 5.43 μ_B/Mn, approaching the spin-only moment 5.91 μ_B per metal calculated from the equation

$$\mu_{eff} = [g^2 S(S+1)]^{1/2} \tag{8}$$

for $S = {}^5/_2$ ions, to a value of 3.0 μ_B/Mn is indicative of small antiferromagnetic interaction.

According to the crystallographic description of **1b** the isotropic Heisenberg Hamiltonian, assuming that the interaction between the terminal Mn^{II} ions is negligible at 7.116 Å, is

$$H = -2J_1(S_1 \cdot S_2 + S_2 \cdot S_3) + H_{ZEEMAN} \tag{9}$$

where $S_1 = S_2 = S_3 = {}^5/_2$ and the Zeeman term is given by eq 3. According to the standard vector coupling rules, the energy values are obtained by eq 10,where S_T assumes values $S_{13} + S_2$

$$E(S,S_{13}) = -J_1\left[S_T(S_T+1) - S_{13}(S_{13}+1) - \frac{35}{4}\right] \tag{10}$$

... $|S_{13} - S_2|$ and S_{13} assumes values $S_1 + S_3$ ... $|S_1 - S_3|$. Using a mean field correction because of intermolecular hydrogen bonding (see text) we fit eq 4 to the susceptibility data. The obtained parameters are $J_1 = -1.9$ cm^{-1}, $g = 2.02$, and $zJ = -0.1$ cm^{-1}, with $R = 0.0013$ where

$$R = \sum_n [(\chi_M)_{exptl} - (\chi_M)_{calcd}]^2 \tag{11}$$

The energy scheme of the compound **1b** is shown in Figure 5A and the ground state is

$$|S_2 = {}^5/_2,\ S_{13} = 5,\ S = {}^5/_2\rangle$$

having the first excited

$$|S_2 = {}^5/_2,\ S_{13} = 4,\ S = {}^3/_2\rangle$$

at $5|J|$ and the second

$$|S_2 = {}^5/_2,\ S_{13} = 5,\ S = {}^7/_2\rangle$$

at $7|J|$. Taking into account the relative weakness of the magnetic interaction between the Mn^{II} ions, an alternative way to determine the J exchange is from the magnetization data. The magnetization curve up to 5 T at 4.0 K is close to a Brillouin function with $S = {}^5/_2$ (Figure 8). Using a modified magnetization model according to Menage et al.[56] we considered that at 4 K and in the 0−5 T field range, the populated spin states are

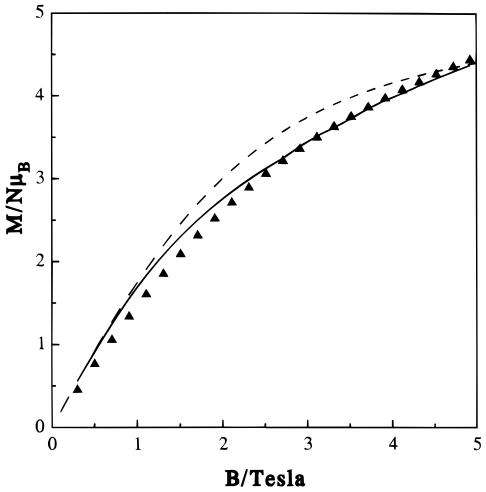

Figure 8. Molar Magnetization M in μ_B vs field B in Tesla. The segmented line represents the theoretical curve for an $S = {}^5/_2$ state, and the solid line is the modified magnetization model (eq 12).

$$|S_2 = {}^5/_2,\ S_{13} = 5,\ S = {}^5/_2,\ M_s\rangle$$

and

$$|S_2 = {}^5/_2,\ S_{13} = 4,\ S = {}^3/_2,\ M_s\rangle$$

It seems quite important to note that other excited states, which were used by Menage et al. in a similar modified magnetization model, are excluded here because they were not stabilized at this field range. The modified magnetization equation is given by

$$M = (Ng\mu_B/2)\left(\frac{dZ}{\frac{d\chi}{Z}}\right) \tag{12}$$

where $Z = Z_{3/2} + Z_{5/2}$ and $\chi = g\mu_B B/\kappa T$. The best fit was obtained for $J = -1.8(1)$ cm^{-1} and $g = 2.04$, in very good agreement with the values from the magnetic susceptibility data, and is shown in Figure 7 too.

ESR Study of 1b. At helium temperature the solid state powder ESR of **1b** exhibits a broad signal centered at $g = 2.0$ with weak features at $g = 4.5$ and $g = 6.5$. The weak features disappear around 20.0 K. Due to the broadness of the signal a temperature dependence study of the intensity and the line width was carried out in order to examine the Curie or non-Curie behavior of the compound. Analogous examination have been carried out by several research groups working on photosystem (PS) II enriched membranes[6−12] and then seem to be of enormous importance[57] in the attempt to explain the appearance of signals such as the $g = 4.1$ and $g = 2.0$ signals.

The temperature dependence of the intensity of the signal $g = 2.0$ is shown in Figure 9, and the ESR spectra at various temperatures is shown in Figure 10. The intensity of the signal was calculated by integration of it in the magnetic field range 2000−5000 G. It increases continuously below 60 K, passing through a maximum at ∼8.0 K followed by a small decrease till 4 K. The small decrease at temperatures below 8.0 K is probably due to antiferromagnetic intermolecular interactions.

(56) Ménage, S.; Vitols, S. E.; Bergcrat, D.; Codjovi, E.; Kahn, O.; Girerd, J. J.; Quillot, M.; Solans, X.; Calvet, T. *Inorg. Chem.* **1991**, *30*, 2666.
(57) Hansson, Ö.; Aasa, R.; Vänngard, T. *Biophys. J.* **1987**, *51*, 825.

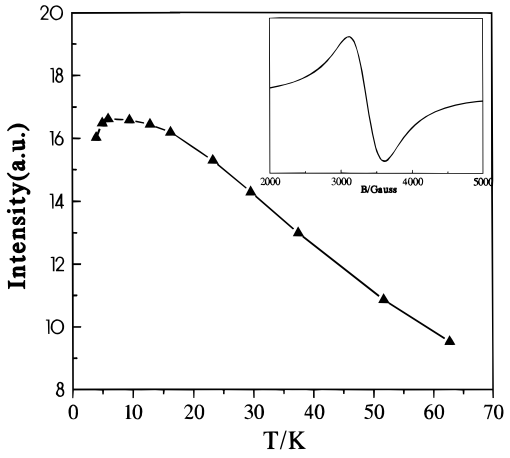

Figure 9. Temperature dependence of the intensity of the signal $g = 2$ (inset) over the field range 2000−4500 G for compound **1b**.

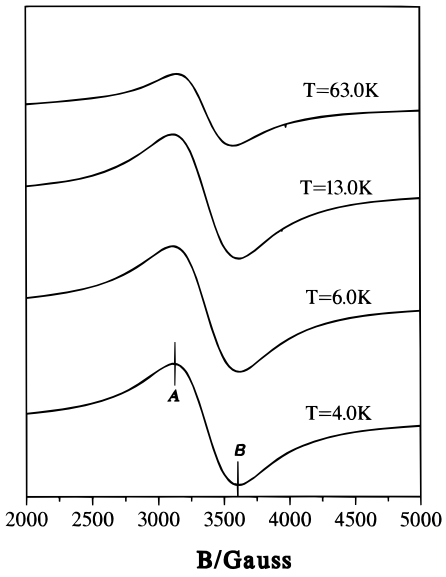

Figure 10. Powder ESR spectra of **1b** at various temperatures. The line width of the signal $g = 2.0$ is $\Delta H = B - A$.

This assumption was used in the interpretation of the magnetic data of **1b** and it was based on the existence of the strong intermolecular hydrogen bonds. Similar behavior of the intensity at low temperatures because of antiferromagnetic intermolecular interaction has been noticed in other complexes as well.[58,59]

The temperature dependence of the ESR line width of the g = 2.0 signal is shown in Figure 11. Generally, the ESR line width for temperatures well above the critical one follows an $1/\kappa_B\chi T$ law, with χ being the static susceptibility which may be responsible for the temperature dependence of ΔH. In the present case the line width reveals a similar behavior with the intensity and the $(\Delta H)^{-1}(\sim\chi T)$ temperature dependence clearly shows the non-Curie variation of the signal (Figure 11). At low temperatures (until 8.0 K) it reveals a plateau, which exhibits the stabilization of the ground state, and then increases with temperature. This is the magnetic behavior for all the Mn^{II}-$Mn^{II}Mn^{II}$ compounds that have been studied until now and reveals the small antiferromagnetic character. The magnitude of the antiferromagnetic interaction is further confirmed by the

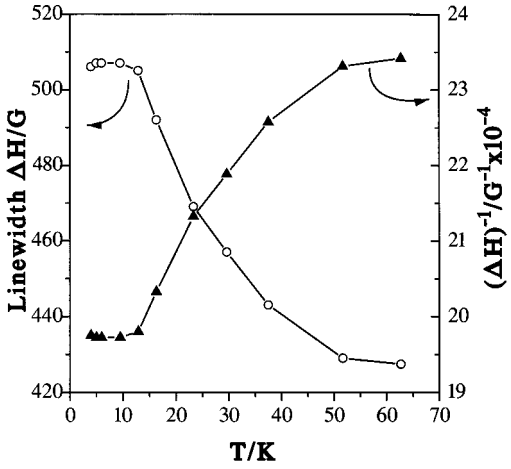

Figure 11. Temperature dependence of the line width ΔH (left axis) and the inverse of ΔH (right axis) for compound **1b**.

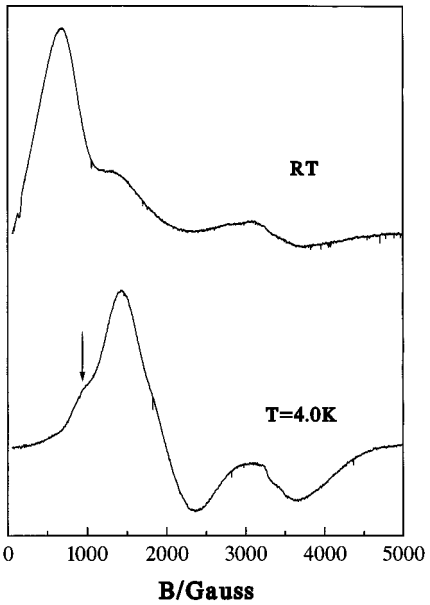

Figure 12. Powder ESR spectra of **3a** at helium and at room temperatures.

small but steady increase of the line width upon cooling, which is evidence of a small interaction.

ESR Study of 3a. The powder ESR spectra of the compound **3a** at helium temperature exhibits a broad low field signal at $g = 4.8$ indicating an $S = {}^3/_2$ ground state (Figure 12). It also exhibits a shoulder at $g = 6.7$, which is an indication of an admixture[60] with the excited state $S = {}^5/_2$, and a signal at $g = 2.0$ with poor intensity. The signal at the low field region grows in until $T = 30$ K. At room temperature a new signal at $g = 9.7$ appears with a weak feature at $g = 4.3$ and $g = 2.0$. Because of the fact that all the states are populated at room temperature it is quite difficult to indicate the origin of it. Temperature dependent population interconversion has also been observed for binuclear $Mn^{III}Mn^{IV}$ models,[58] behavior which has been suggested as the origin of the two S_2 state ESR spectral signatures.

In CH_2Cl_2 glass a very broad signal centered at $g = 4.3$ appears, which strongly indicates an $S = {}^3/_2$ state, while a signal at $g = 2.0$ with more than six lines is observed (Figure 13). We should mention that the temperature dependence of the ESR spectrum reveals that the intensity of the signal at $g = 4.3$ and

(58) Larson, E. J.; Haddy, A.; Kirk, M. L.; Sands, R.; Hatfield, W. E.; Pecoraro, V. L. *J. Am. Chem. Soc.* **1992**, *114*, 6263.
(59) Gouskos, N.; Likodimos, V.; Londos, C. A.; Psycharis, V.; Mitros, C.; Koufoudakis, A.; Gamari-Seale, H.; Windsch, W.; Metz, H. *J. Solid State Chem.* **1995**, *119*, 50.
(60) Philouze, G.; Blondin, G.; Girerd, J. J.; Guilhen, J.; Pascard, C.; Lexa, D. *J. Am. Chem. Soc.* **1994**, *116*, 8557.

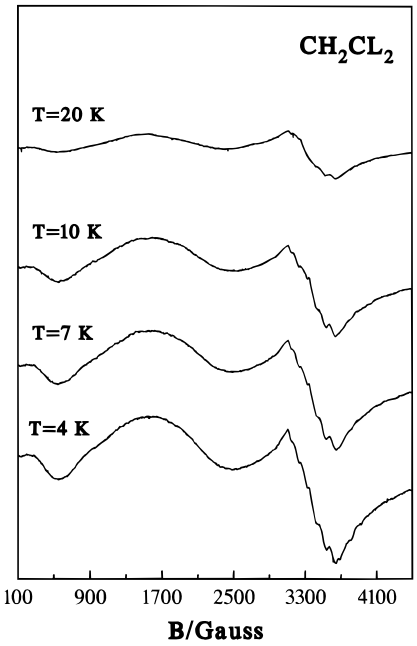

Figure 13. X-band ESR spectra of **3a** as a CH_2Cl_2 glass at various temperatures.

$g = 2$ decreases when the temperature is decreased. This agrees well with the electric conductance measurements of CH_2Cl_2 solutions of **3a**. In addition hyperfine structure is observed in the $g = 4.3$ signal which is in line with previous reports.[21,22,25]

The ESR spectra in MeOH show a classic six-line signal centered at $g = 2$ from uncomplexed Mn^{II} due to dissociation of the complexes to form monomeric units of $[Mn^{II}(AcO)_2(Hsal)_2]^{2-}$ and $[Mn^{III}saladhp]^+$ as has been shown by an ^1H NMR study.[47] The conductance of MeOH solution indicates that a 2:1 electrolyte is formed.

Conclusion. While mixed- and homo-valence trimers have been reported previously, some very interesting features are presented in this report. The compound **3a**, is the first example of structurally characterized mixed-valence trimer that has on the sixth position of the terminal manganese atoms a neutral ligand without an $-OH$ group, a fact which allows the certain assignment of the oxidation state of it as Mn^{III}. It is also the first example which by showing an inter- and intra-H-bond network justifies the use of a mean field correction for the interpretation of magnetic data. A new approach to the interpretation of the magnetic behavior of this homovalence trinuclear class of compounds is also presented. The exchange parameter was obtained from the magnetization data with a modified magnetization equation assuming that the populated states at 4 K are $|S_2 = {}^5/_2, S_{13} = 5, S = {}^5/_2, M_s\rangle$, $|S_2 = {}^5/_2, S_{13} = 4, S = {}^3/_2, M_s\rangle$. Finally it is reported for the first time that an ESR study of such mixed-valence compounds at various temperatures shows a multiline signal ($g = 2$) at low temperature (4 K) related to the trimer, while the study in the solid state shows a temperature dependent population interconversion for the low field signal. The study of the ESR spectra of Mn^{II}_3 at various temperatures in a manner analogous to the study of PS-II enriched membranes gave important information concerning the antiferromagnetic character of the compound as well as the behavior of it at low temperatures (intermolecular interactions). Its results are in accordance with the magnetic measurements for this compound, and this clearly provides an efficient experimental methodology for studying the magnetic behavior of analogous compounds.

Acknowledgment. This work was supported by the Greek Ministry of Industry, Energy and Technology, General Secretariat of Research and Technology (PENED91). V.T. and A.T. thank Mrs. A. Athanassiou for financial support.

Supporting Information Available: Two X-ray crystallographic files, in CIF format, are available. Access information is given on any current masthead page.

IC960183J